

## Interleaved Boost Converter For Photovoltaic Power-Generation System

Suguna.J<sup>[1]</sup>, kathiravan.A<sup>[2]</sup>, VimalRaj.P<sup>[3]</sup>,  
<sup>1,2,3</sup>Christ College Of Engineering and Technology

---

**Abstract:** in this paper, an interleaved boost converter (IBC) for a photovoltaic (PV) power-generation system is proposed. The topology used raises the efficiency of the DC/DC converter of the PV power conditioning system (PVPCS), and it minimizes switching losses by adopting a resonant soft-switching method. A detailed mode analysis of the proposed topology is presented. Consequently, it is confirmed that the overall efficiency is increased by about 1.5% compared with the conventional hard switching interleaved boost converter.

**Index Terms:** Boost converter, interleaved, maximum power point tracking (MPPT), photovoltaic (PV) power-generation systems, resonant converter, soft-switching.

---

### I. Introduction

RECENTLY, photovoltaic (PV) energy has attracted interest as a next generation energy source capable of solving the problems of global warming and energy exhaustion caused by increasing energy consumption. PV energy avoids unnecessary fuel expenses and there is no air pollution or waste. Also, there are no mechanical vibrations or noises because the components of power generation based on PV energy use semiconductors. The life cycle of the solar cell is more than 20 years, and it can minimize maintenance and management expenses. The output power of the solar cell is easily changed by the surrounding conditions such as irradiation and temperature, and also its efficiency is low. This high efficiency is required for the power conditioning system (PCS), which transmits power from the PV array to the load. In general, a single-phase PV PCS consists of two conversions Stages (i.e., DC/DC conversion stage and DC/AC conversion stage). The DC/DC converter is the first stage and it performs maximum power-point tracking (MPPT) and Guarantees the DC-link voltage under low irradiance conditions [1], [2]. This paper proposes a high efficiency DC/DC boost converter to Increase the overall efficiency of the PV power conditioning system (PVPCS) [3]–[8]. We studied a 2-phase interleaved boost converter integrated with a single-switch type soft-switching boost converter. The proposed single-switch type soft-switching boost converter can minimize switching losses by adopting a resonant soft-switching method. And, no additional switches are needed for soft switching [9]–[15]. However, the drawback of this converter is that the voltage across the switch is very high during the resonance mode. The voltage across the switch depends on the parameters of the resonant components (i.e., resonant inductance and resonant capacitance) and the resonant inductor current. In this paper, the optimal design of the resonant components and the interleaved method is applied for resonant current reduction. Since the interleaved method distributes the input current according to each phase, it can decrease the current rating of the switching device. Also, it can reduce the input current ripple, output voltage ripple, and size of the passive components [16]–[18]. The proposed soft-switching interleaved boost converter can not only exploit the interleaved converter, but also reduce switching losses through the soft-switching technique. Therefore, the output power of the PV array can be boosted with high efficiency. This paper presents the operational principle of the converter, for simulated.

### II. Proposed Topology

#### A. Proposed Soft-Switching Boost Converter

The interleaved boost converter consists of two single-phase Boost converters connected in parallel. The two PWM signal The difference is 180° when each switch is controlled by the interleaving method. Because each inductor current magnitude is decreased according to one per phase, we can reduce the inductor size and inductance when the input current flows through two boost inductors. The input current ripple is decreased because the input current is the sum of each current of inductor L1 and L2 .Fig. 1(a) shows the proposed single-switch type soft switching boost converter [19]. One resonant inductor, two capacitors, and two diodes are added to a conventional boost converter for soft switching using resonance. Fig. 1(b) shows the interleaved soft-switching boost converter (ISSBC) proposed in This paper. Two single-phase soft-switching boost converters are connected in parallel and then to a single output capacitor.

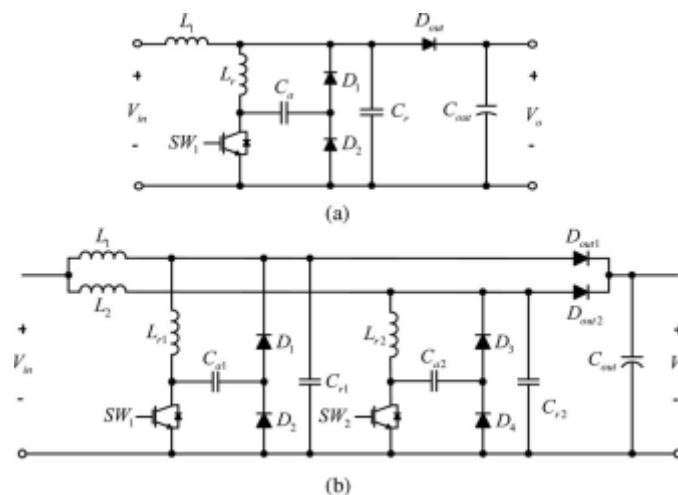


Fig. 1 Proposed soft-switching boost converter. (a) Proposed single-switch soft-switching boost converter.(b) ISSBC

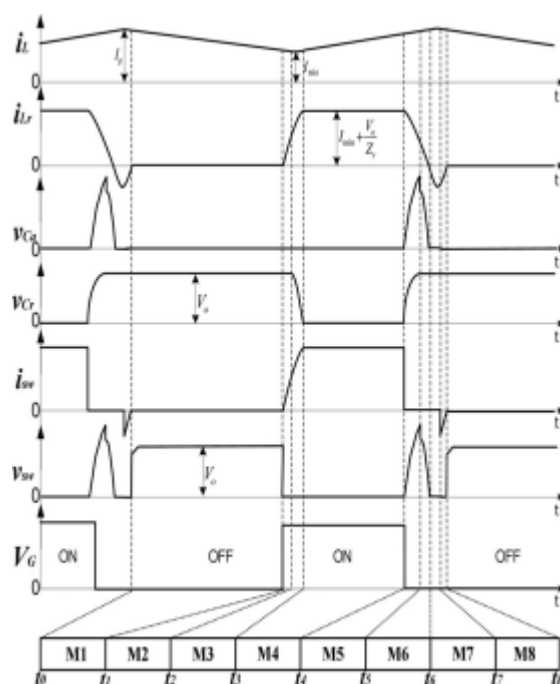


Fig. 2. Key waveforms of proposed converter.

**B. Mode Analysis of the Proposed Converter**

Each mode is presented during one switching cycle of steady state operation of the proposed converter. For illustrating the soft-switching operation using resonance, we describe the operation modes of a single-phase soft switching boost converter [see Fig. 1(a)], which consists of the proposed ISSBC. The key waveforms associated with the operation stages are shown in Fig. 2. There are operation modes shown in Fig. 3, and the duty ratio is assumed to be 0.5 in order to simplify the analysis. The operation can be analyzed in terms of eight modes according to the operating conditions defined in the following paragraphs.

- 1) All switching devices and passive elements are ideal.
- 2) The parasitic components of all switching devices and Elements are ignored.
- 3) It is assumed that the initial value of operation mode is equal to zero.

**Mode 1 ( $t_0 \leq t < t_1$ ):** The switch is in the off state and the DC Output of the solar cell array is transmitted directly to the load Through L and D<sub>out</sub>. In this mode, the main inductor voltage Becomes ( $V_o - V_{in}$ ). Thus, the main inductor current decreases linearly

$$iL(t) = iL(t_0) - \frac{V_o - V_{in}}{L} t \quad (1)$$

$$iL_r(t) = 0, \quad vCr(t) = V_o, \quad vCa(t) = 0 \quad (2)$$

$$iL(t_1) = I_1 \quad (3)$$

**Mode 2 ( $t_1 \leq t < t_2$ ):** In mode 2, the switch is turned on under Zero-current switching (ZCS) because of the resonant inductor  $L_r$ . In this case, as the output voltage is supplied to the resonant inductor  $L_r$ , the current increases linearly. When the resonant current  $iL_r$  becomes equal to the main inductor current  $I_L$ , the current of the output side diode  $D_{out}$  becomes zero

$$iL = I_1 - \frac{V_o - V_{in}}{L} t \quad (4)$$

$$iL_r(t) = \frac{V_o}{L_r} t, \quad vCr(t) = V_o, \quad vCa(t) = 0 \quad (5) \quad iL(t_2) = I_{min}, \quad iL_r(t_2) = I_{min} \quad (6)$$

**Mode 3 ( $t_2 \leq t < t_3$ ):** When the output current  $iD_{out}$  becomes zero, the mode starts. In this mode, the resonant inductor  $L_r$  and the resonant capacitor  $C_r$  resonate and the voltage of  $C_r$  decreases from the output voltage  $V_o$  to zero. In this case, the main inductor current  $I_L$  flows through  $L_r$  and the switch

$$iL(t) = I_{min} \quad (7)$$

$$V_{C_a}(t) = 0 \quad (8)$$

$$iL_r(t) = I_{min} + \frac{V_o}{Z_r} t \quad (9)$$

$$V_{C_r}(t) = V_o \cos \omega r t \quad (10)$$

$$iL_r(t_3) = I_2, \quad vCr(t_3) = 0 \quad (11)$$

$$\omega r = \frac{1}{\sqrt{L_r C_r}}, \quad Z_r = \sqrt{L_r C_r} \quad (12)$$

**Mode 4 ( $t_3 \leq t < t_4$ ):** When the resonant capacitor voltage  $V_{C_r}$  becomes zero, the two auxiliary diodes  $D_1$  and  $D_2$  are turned on and the mode starts. In this mode, the resonant inductor current is separated into two parts. One is the main inductor current  $iL$  and the other is the current turning through the two auxiliary diodes. The main inductor current  $iL$  increases linearly

$$L(t) = I_{min} + \frac{V_{in}}{L} t \quad (13)$$

$$iL_r(t) \approx I_2 \quad (14)$$

$$V_{C_r}(t) = 0, \quad V_{C_a}(t) = 0 \quad (15)$$

$$iL(t_4) = I_3, \quad iL_r(t_4) = I_2 \quad (16)$$

**Mode 5 ( $t_4 \leq t < t_5$ ):** In mode 5, the switch turns off under The zero-voltage condition because of the auxiliary resonant capacitor  $C_a$ . There are two current loops. One is the  $L$ - $C_r$  -  $V_{in}$  loop for which the voltage of the resonant capacitor  $C_r$  increases linearly from zero to the output voltage  $V_o$ . The other is the  $L_r$ - $C_a$ - $D_1$  loop for which the second resonance occurs. The energy stored in  $L_r$  is transferred to  $C_a$ . The resonant current  $iL_r$  decreases linearly and the voltage across  $C_a$  becomes maximum.

$$iL(t) \approx I_3 = I_{ma} \quad (17)$$

$$iL_r(t) = I_2 \quad (18)$$

$$V_{C_a}(t) = Z_r I_2 \sin \omega a t, \quad V_{C_r}(t) = I_2 / C_a \quad (19)$$

$$\omega a = 1 / \sqrt{L_r C_a} \quad (20)$$

$$Z_a = \sqrt{L_r / C_a} \quad (21)$$

**Mode 6 ( $t_5 \leq t < t_6$ ):** When the resonant capacitor voltage  $v_{C_r}$  is equal to the output voltage  $V_o$ , the mode starts. In this mode, the energy flow from  $L_r$  to  $C_a$  is completed and the resonant current  $iL_r$  becomes zero

$$iL(t) = I_3 - \frac{V_o - V_{in}}{L} t \quad (22)$$

$$iL_r(t) = I_2 \cos \omega a t \quad (23)$$

$$vCa(t) = Z_r I_2 \sin \omega a t, \quad vCr(t) = V_o \quad (24)$$

$$vCa(t_6) = Z_a I_2 \quad (25)$$

**Mode 7 ( $t_6 \leq t < t_7$ ):** In mode 7, the voltage of  $C_a$  decreases, continuously resonates on the  $D_2$ - $C_a$ - $L_r$ - $D_{out}$ - $C_o$  loop and the energy is transferred from  $C_a$  to  $L_r$ . When the  $C_a$  voltage becomes zero, the resonant current  $iL_r$  is the reverse of the current direction of mode 6. When the voltage of  $C_a$  becomes zero, the anti-parallel diode of the switch turns on and it transitions conditions..

$$iL(t) = I_3 - \frac{V_o - V_{in}}{L} t, iLr(t_6) = I_4 \quad (26)$$

$$iLr(t) = \left(\frac{V_o}{Z_a} - I_2\right) \sin \omega a t, iLr(t) = I_5 \quad (27)$$

$$vCr(t) = V_o \quad (28)$$

$$vCa(t) = V_o - (V_o - Z_a I_2) \cos \omega a t = V_2 \quad (29)$$

**Mode 8 ( $t_7 \leq t < t_8$ ):** There are two current loops. The main inductor current  $iL$  transmits energy to the output through  $D_{out}$  and decreases linearly. The resonant inductor current  $iLr$  also transmits energy to the load through  $D_{out}$  and flows through the antiparallel diode of the switch. When the resonant inductor current  $iLr$  becomes zero, mode 8 ends

$$iL(t) = I_4 + \frac{V_o - V_{in}}{L} t, iLr(t_8) = I_6 \quad (30)$$

$$iLr(t) = I_5 - \frac{V_o}{Lr} t, iLr(t_8) = 0 \quad (31)$$

$$vCr(t) = V_o \quad (32)$$

$$vCa(t) = 0 \quad (33)$$

**TABLE I**  
**Experimental Parameters**

Parameter	Symbol	value	unit
Input voltage	$V_{in}$	180-200	V
Output voltage	$V_o$	400	V
Rated power	$P_o$	1.2	KW
Switching frequency	$f_{sw}$	30	KHz
Main inductor	$L_1, L_2$	1	mH
Resonant inductor	$L_{r1}, L_{r2}$	50.6	$\mu$ H
Resonant capacitor	$C_{r1}, C_{r2}$	100	nF
Auxiliary capacitor	$C_{a1}, C_{a2}$	10	nF
Output capacitor	$C_{OUT}$	15	$\mu$ F

### III. Design Procedures Of The Proposed Converter

#### A. Switch Peak Voltage Analysis and Parameter Design

In mode 5, the current that flows through the  $L_r$ - $Ca$ - $D1$  loop the next mode Should be large enough for resonance. As described by (18), the voltage across the auxiliary resonant capacitor  $C_{a1}$  as high as  $I_2$  during this resonant period. Voltage across the auxiliary resonant capacitor  $C_{a1}$  as high as  $I_2$  during this resonant period

$$v_{SW}(t) = v_{Ca}(t) + v_{Cr}(t)$$

The amplitude of the switch voltage is determined by the resonant devices and the resonant current. To minimize the peak voltage of the switch, designs for optimal parameters of resonant components are included and the interleaved method is adopted. Because the interleaved method distributes the input current according to each phase, it can decrease the current rating of the switching device. Thus, it can reduce the peak voltage across the switch, input current ripple, output voltage ripple and size of passive components.

#### B. Selection of Resonant Inductor and Capacitor

The ZVS condition of the switch is affected by the auxiliary Resonant capacitor  $Ca$ . In mode 5, the current that flows through the  $L_r$ - $Ca$ - $D1$  loop should be large enough for resonance. In general, the snubbed capacitance has to be more than ten times the parasitic capacitance. The resonant capacitance  $Ca$  has to be more than 20 times the output capacitance of the switch, because the  $C_{a1}$  charged by the resonant inductor current (it is about 2 times the main inductor current) during the switch turn-off period, represented as follows:  
 $C_a > 20 C_{oes}$ .

In mode 3, the resonant inductor current is represented by (8). The period of resonance between resonant inductance  $L_{rand}$  Resonant capacitance  $Cr$  is about a quarter of the entire resonant period. In general, the rising time of the resonant inductor current is 10% of the minimum on-time of the switch. However  $r$ , for satisfaction of the ZVS condition, the rising time of the resonant inductor current is 50% of the minimum on-time in this paper, as represented by

$$T_3 - T_1 = \frac{Lr}{V_o} I_{min} + \frac{Tr}{4} < 0.5 D_{min} T \quad (34)$$

Where

$$Tr = \frac{1}{fs} = 2\pi\sqrt{LrCr}$$

$$Tr = \frac{1}{fsw}$$

And  $D_{min} = (Vo - Vin_{min})/Vo$ .

From (18) and (25), the resonant capacitance Cr can be defined as

$$Cr > \frac{D^{2min}}{\pi^2 Lr f^2 sw} + \frac{I^2 min Lr}{\pi^2 Vo^2} - \frac{2Imin Dmin}{\pi^2 Vo fsw^2} \quad (35)$$

Since  $(2Imin Dmin)/(\pi^2 Vo fsw^2) \approx 0$  in (36), this equation can be rewritten as follows:

$$Cr > \frac{D^{2min}}{\pi^2 Lr f^2 sw} + \frac{I^2 min Lr}{\pi^2 Vo^2}$$

$$Lr = \{Vo(I2 - Imin)\}^2 Cr$$

Where  $I2 - Imin = Vo/Zr = Vo\sqrt{Cr} / \sqrt{Lr}$

From (37) and (38), Cr can be defined as

$$Cr > \frac{D^{2min}(I2 - Imin)}{\pi^2 Lr f^2 sw} / \sqrt{I - I^2 min / \pi^2 (I2 - Imin)^2} \quad (36)$$

From (38), the resonant inductor parameter is expressed as

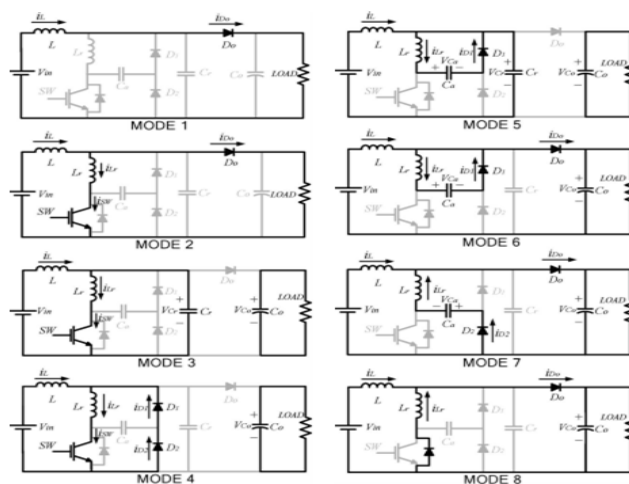
$$Lr < \left\{ 2 \times 0.85 \frac{Cs}{Ca} - Vo \left( \frac{If}{Cr + Ca} \pi \sqrt{Ca} \right)^2 \right\}$$

Where

$$Cs = Cr Cs / (Cr + Ca), \quad Vo - V2 \approx 0.85Vo$$

### C. Design Example

In this section, the design procedure of the proposed converter is based on the derived equations. Table I shows the Design parameters of the proposed boost converter. And, the Design guidelines herein provides a proper tool to help choose resonant components and ensure the appropriate operation of the resonance converter.



#### IV. Simulation Results

##### A. Simulation diagram for Interleaved Boost Converter

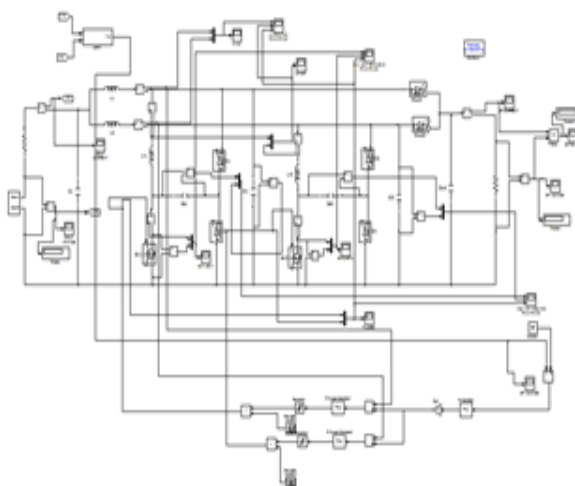


Fig 1 Simulation diagram of Interleaved Boost Converter

##### B. MPPT Controller: P&O MPPT Algorithm

The MPPT algorithm used in the simulations is a hill climbing P&O technique. The boost converter duty ratio is changed and the resulting change in power is observed. The duty ratio is then changed again based on the previous sample such that the new duty ratio is closer to the MPP. In this simulation, the boost converter duty ratio and the average power generated by the PV are measured and compared to the value during the previous sample. The sample rate is 100Hz. The change in duty ratio and change in average power are multiplied together and then compared to zero. If the product is positive, the duty ratio is incremented by 1%. If the product is negative, the duty ratio is decremented by 1%. If the product is zero, the control toggles between incrementing and decrementing the duty ratio by 1%. This prevents the simulation from getting stuck at one duty ratio, and does not appear to add additional oscillation around the equilibrium point. The duty ratio is limited between 0 and 90% to keep the boost converter in a suitable operating range.

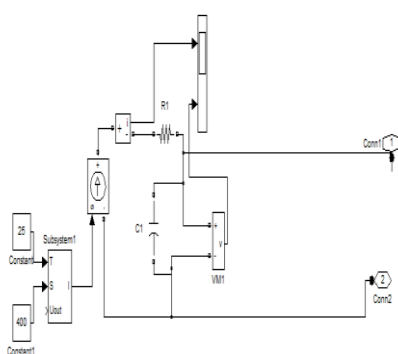


Fig .2 Simulation model of PV array

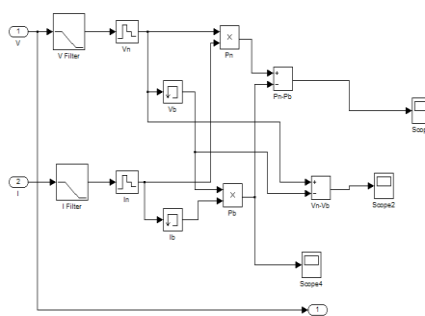


Fig .3 Simulink model of P&O MPPT converter control

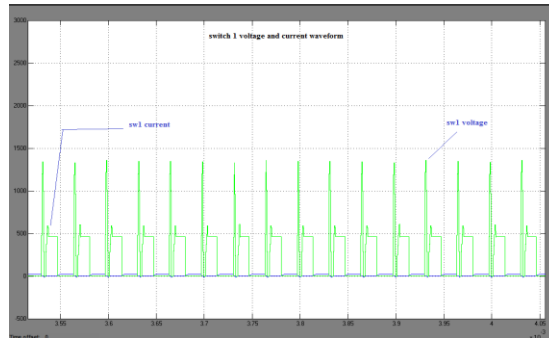


Fig.4 Simulation result for sw1 current and voltage

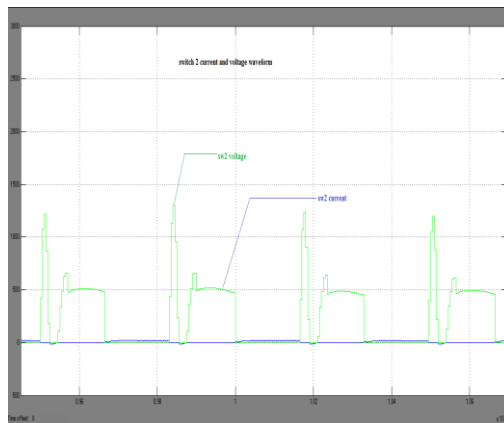


Fig.5 Simulation result for sw2 current and voltage

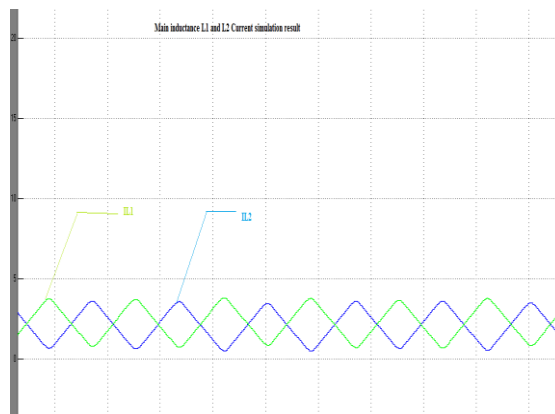


Fig.6 Simulation result for main inductance current

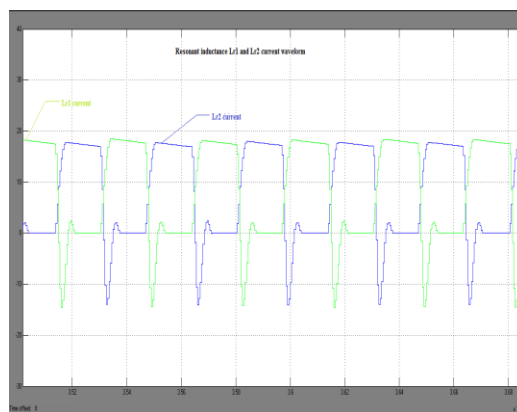


Fig. 7 Simulation result for resonant inductance current

Fig.6&7 shows the current waveforms of the resonant inductor Lr1,Lr2 , and gate signals. The current through Lr1 and Lr2 are more than twice the main inductor L1 and L2 current

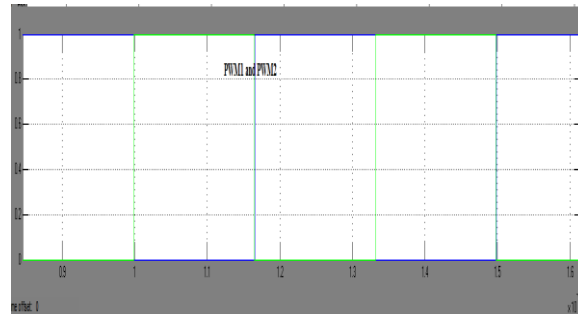


Fig.8 Simulation result for PWM 1 and PWM 2



Fig. 9 Simulation result for MPPT pulses

Fig.9 shows the MPPT Pulses of the system the constant level of the pulses given to the system the perfect output is produced.

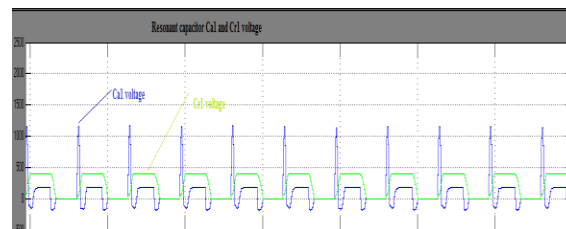


Fig.10 Simulation result for resonant capacitor Ca1 and Cr1 voltage

Fig.10 shows the Ca1 and Ca2 of resonant

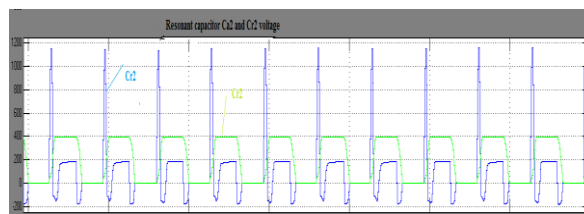


Fig.11 Simulation result for resonant capacitor Ca2 and Cr2 voltage

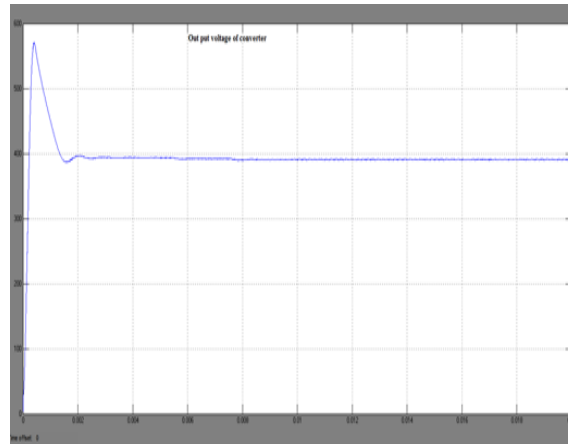


Fig.12simulation result for converter output voltage

Fig. 12 shows the output voltage waveform of the converter to produce twice amount of voltages produced.

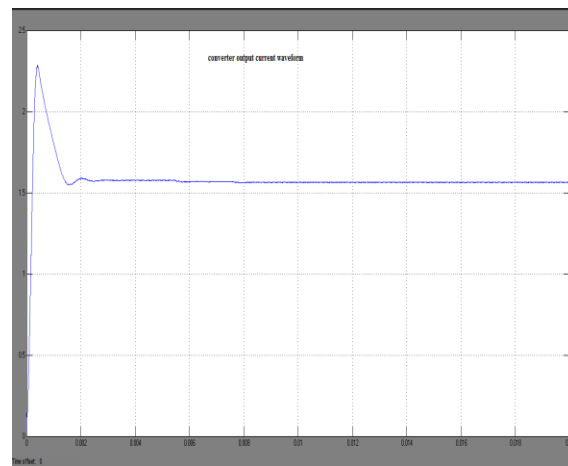


Fig.13Simulation result for converter output current

Fig. 13 shows the output current of the converter to produced constant current of the system.

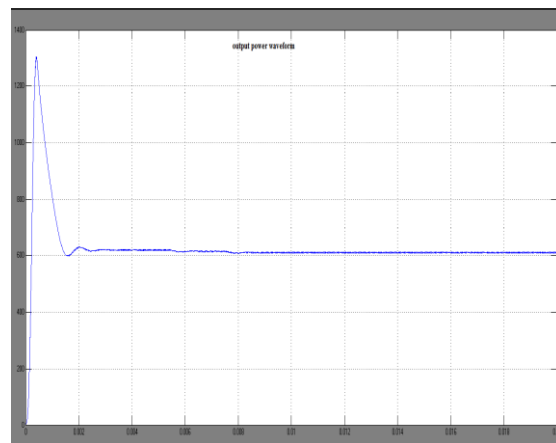


Fig. 14 Simulation result for converter output power

Fig. 14 shows the output power of the converter multiple product of the voltage and current the power is developed so constant amount of power is obtained.

The MATLAB simulation software was used to analyse theOperational characteristics of the proposed soft-switching interleaved boost converter. The design parameters for the simulationare shown in Table I.Fig.4&5 shows the current waveforms of the main inductor and resonant inductor, and the gate signals (SW1

and SW2) of the proposed soft-switching interleaved boost converter. The main inductor currents ( $i_{L1}$  and  $i_{L2}$ ) increase and decrease linearly according to the gate signals. The phase difference of each waveform is  $180^\circ$ . Also, the resonant inductors store and release energy according to the gate signals. Fig. 6 shows the voltage waveforms of the resonant capacitor and auxiliary resonant capacitor, and gate signals (SW1 and SW2). The peak voltage of  $V_{Ca1}$  is higher than that of the resonant capacitor voltage  $V_{Cr}$ . When the switch turns off, the auxiliary resonant capacitor voltage  $V_{Ca2}$  increases and then decreases to the zero level, satisfying the ZVS condition represented by (36). Fig. 7 shows the voltage and current waveforms of the switches and gate signals. The switches SW1 and SW2 are turned on under ZCS and turned off under ZVS.

## V. Conclusion

The interleaved boost and converter with both zero-voltage switching and zero-current-switching functions and a closed loop control system has been designed for the ZCS Interleaved boost converter in continuous time domain using the PID controller. The simulation results thus obtained using MATLAB/Simulink is proposed in this paper. The duty cycle of this topology can be more or less than 30% reused each switches.

- 1) The main switches Sw1 and Sw2 can achieve both ZVS and ZCS.
- 2) The voltage stress of all switches are reduced by using soft switching techniques.
- 3) It uses the resonant inductor  $L_r$ , resonant capacitor  $C_r$ , Parasitic capacitors  $C_{a1}$  and  $C_{a2}$ ,
- 4) The driving circuit can automatically detect whether the Driving signals of the main switches are more than 50% or not and get the driving signal of the auxiliary switch.
- 5) The users can only apply the ZVS or ZCS function just By the adjustment of the driving circuit
- 6) The efficiency is 97.6% with output voltage is 400 and input voltage of 150V to 200V and it is 97.6% with output power is obtained.

## References

- [1]. Interleaved Soft-Switching Boost Converter for Photovoltaic Power-Generation System Doo-Yong Jung, Young-Hyok Ji, Sang-Hoon Park, Yong-Chae Jung, and Chung-Yuen Won, Senior Member, IEEE
- [2]. J.-P. Lee, B.-D. Min, T.-J. Kim, D.-W. Yoo, and J.-Y. Yoo, "Design and control of novel topology for photovoltaic dc/dc converter with high efficiency under wide load ranges," *J. Power Electron.*, vol. 9, no. 2, pp. 300–307, Mar. 2009.
- [3]. B.-D. Min, J.-P. Lee, and J.-H. Kim, "A novel grid-connected PV PCS with new high efficiency converter," *J. Power Electron.*, vol. 8, no. 4, pp. 309–316, Oct. 2008.
- [4]. G. Hua, C.-S. Leu, Y. Jiang, and F. C. Y. Lee, "Novel zero-voltage transition PWM converters," *IEEE Trans. Power Electron.*, vol. 9, no. 2, pp. 213–219, Mar. 1994.
- [5]. G. Hua, E. X. Yang, Y. Jiang, and F. C. Y. Lee, "Novel zero-current transition PWM converters," *IEEE Trans. Power Electron.*, vol. 9, no. 6, pp. 601–606, Nov. 1994.
- [6]. H. Bodur and A. F. Bakan, "A new ZVT-ZCT-PWM DC-DC converter," *IEEE Trans. Power Electron.*, vol. 19, no. 3, pp. 676–684, May 2004.
- [7]. H. Bodur and A. F. Bakan, "A new ZVT-PWM DC-DC converter," *IEEE Trans. Power Electron.*, vol. 17, no. 1, pp. 40–47, Jan. 2002.
- [8]. N. Jain, P. K. Jain, and G. Joos, "A zero voltage transition boost converter employing a soft switching auxiliary circuit with reduced conduction losses," *IEEE Trans. Power Electron.*, vol. 19, no. 1, pp. 130–139, Jan. 2004.
- [9]. S. K. Kwon and K. F. A. Sayed, "Boost-half bridge single power stage PWM DC-DC converters for PEM-fuel cell stacks," *J. Power Electron.*, vol. 8, no. 3, pp. 239–247, Jul. 2008.
- [10]. X. Kong and A. M. Khambadkone, "Analysis and implementation of a high efficiency, interleaved current-fed full bridge converter for fuel cell system," *IEEE Trans. Power Electron.*, vol. 22, no. 2, pp. 543–550, Mar. 2007.
- [11]. H. M. Suryawanshi, M. R. Ramteke, K. L. Thakre, and V. B. Borghate, "Unity-power-factor operation of three-phase ac-dc soft switched converter based on boost active clamp topology in modular approach," *IEEE Trans. Power Electron.*, vol. 23, no. 1, pp. 229–236, Jan. 2008.
- [12]. H. Mao, O. Abdel Rahman, and I. Batarseh, "Zero voltage-switching dc-dc converters with synchronous rectifiers," *IEEE Trans. Power Electron.*, vol. 23, no. 1, pp. 369–378, Jan. 2008.
- [13]. H. Tao, A. Kotsopoulos, J. L. Duarte, and M. A. M. Hendrix, "Transformer-coupled multiport ZVS bidirectional dc-dc converter with wide input range," *IEEE Trans. Power Electron.*, vol. 2, pp. 771–781, Mar. 2008.

- [14]. H. Xiao and S. Xie, "A ZVS bidirectional dc–dc converter with phase-shift plus PWM control scheme," *IEEE Trans. Power Electron.*, vol. 23, no. 2, pp. 813–823, Mar. 2008.
- [15]. D. V. Ghodke, K. Chatterjee, and B. G. Fernandes, "Three-Phase threelevel, soft switched, phase shifted PWdc-dc converter for high power applications," *IEEE Trans. Power Electron.*, vol. 23, no. 3, pp. 1214–1227, May 2008.
- [16]. M. Borage, S. Tiwari, S. Bhardwaj, and S. Kotaiah, "A full-bridge dc–dc converter with zero-voltage-switching over the entire conversion range," *IEEE Trans. Power Electron.*, vol. 23, no. 4, pp. 1743–1750, Jul. 2008.
- [17]. S. Y. Tseng, J. Z. Shiang, H. H. Chang, W. S. Jwo, and C. T. Hsieh, "A novel turn-on/off snubber for interleaved boost converter," *Proc. IEEE 38th Annu. Power Electron. Specialists Conf. (PESC 2007)*, 2718–2724.
- [18]. X. Wu, J. Zhang, X. Ye, and Z. Qian, "Analysis and derivations for a family ZVS converter based on a new active clamp ZVS cell," *IEEE Trans. Ind. Electron.*, vol. 55, no. 2, pp. 773–781, Feb. 2008.
- [19]. P.-W. Lee, Y.-S. Lee, D. K. W. Cheng, and X.-C. Liu, "Steady-state analysis of an interleaved boost converter with coupled inductors," *IEEE Trans. Ind. Electron.*, vol. 47, no. 4, Aug. 2000.
- [20]. D.-Y. Jung, Y.-H. Ji, J.-H. Kim, C.-Y. Won, and Y.-C. Jung, "Soft switching boost converter for photovoltaic power generation system," *Proc. 13th*